

**Water and Environmental Research Center
Annual Technical Report
FY 2016**

Introduction

The University of Alaska Fairbanks Water & Research Center (WERC) provides the State of Alaska with water resource solutions for the challenging Arctic and Subarctic regions. WERC, along with a team of civil and environmental engineers, hydrologists, limnologists, ecologists, chemists, social scientists, permafrost scientists, and an array of other faculty, staff and student researchers, strive to understand the changing environment to improve the quality of life for all Alaskan's while protecting the bountiful natural resources in a fragile ecosystem. WERC is America's Arctic University and continues to be one of our nation's foremost centers of expertise in field based cold regions water research.

Research Program Introduction

The FY2016 104(b) grants continue to reflect the diverse nature of our current research. The 104(b) grants we received for the funding period were instrumental in allowing a group of WERC-affiliated students to pursue research projects important to the State of Alaska. This year's topics include an examination of how lake levels have changed in response to long-term environmental changes, modeling snow melt for use in hydrologic studies forecasting water availability, removal of toxic heavy metals from contaminated water using a metal-organic framework (MOF)-graphene oxide (GO) hybrid material, and a study on the transport of CH₄ through open taliks in discontinuous permafrost aquifers. Each topic examines an area of concern to the State of Alaska and is reflective of the broad nature of research WERC actively pursues.

Transport of CH₄ through Open Taliks in Discontinuous Permafrost Aquifers

Basic Information

Title:	Transport of CH ₄ through Open Taliks in Discontinuous Permafrost Aquifers
Project Number:	2016AK130B
Start Date:	3/1/2016
End Date:	2/28/2017
Funding Source:	104B
Congressional District:	AK-001
Research Category:	Ground-water Flow and Transport
Focus Category:	Groundwater, Solute Transport, None
Descriptors:	None
Principal Investigators:	David L. Barnes

Publications

1. Eckhardt, B.A., Barnes, D.L., Daanen, R.P., Walter Anthony, K.P. (2017). Transport of CH₄ in Thermokarst Lakes in Discontinuous Permafrost. Poster presentation at Week of the Arctic 2017. 10 May 2017, Fairbanks, AK.
2. Eckhardt, B.A., Barnes, D.L., Daanen, R.P., Walter Anthony, K.P. (2016). Transport of CH₄ in Open-Talik Lakes in Discontinuous Permafrost Aquifers. Poster presentation at American Geophysical Union Annual Fall Meeting. 15 December 2016, San Francisco, CA.

TITLE

Transport of CH₄ Through Open Taliks in Discontinuous Permafrost Aquifers

RESEARCH SUMMARY

Objectives

Our project sought to characterize the potential transport mechanisms for methane (CH₄) in the groundwater-to-lake system of two thermokarst lakes in the Goldstream Creek Basin, Fairbanks, Alaska. Our objectives were as follows:

- Determine the potential advective flux of CH₄ through open taliks by measuring vertical pressure gradients and hydrostatic heads.
- Determine the potential diffusive flux of CH₄ through open taliks by measuring dissolved CH₄ concentration gradients.
- Assess the potential for flow of CH₄ as an immiscible fluid in the saturated soils comprising the sub-lake taliks.

Methods/materials

During the Spring of 2016, vibrating wire piezometers and Rhizon soil solution samplers (RSSS) were installed in both lakes below the sediment surface within the sub-lake taliks in order to monitor the direction of groundwater flow and dissolved CH₄ concentration gradient. Three (3) vibrating wire piezometers attached to a single metal pole was installed within the sub-lake taliks of each lake. Five (5) RSSS were installed on a single metal pole that was installed in two locations within the sub-lake taliks of each lake. Drive point wells outfitted with water level loggers were installed in the Summer of 2016 in four (4) locations around each lake to monitor supra-permafrost groundwater flow and to obtain supra-permafrost groundwater samples. Monthly sampling of surface lake water, benthic lake water, sub-lake talik porewater, supra-permafrost groundwater, and residential well groundwater provided water samples for analysis of dissolved CH₄ and stable water isotopes, deuterium and oxygen-18. These samples were later also analyzed for dissolved anions and cations using an ion chromatograph (IC) and an inductively-coupled plasma atomic emissions spectroscopy instrument (ICP-AES). Soil moisture characteristic curves were developed for Goldstream silt and gravel samples using Tempe cells and 5-bar and 15-bar pressure plates in Dr. Margaret Darrow's lab. RETC program and the Brooks and Corey model was used to model the soil moisture characteristic curves of the soils.

Results/discussion

Advection

Figure 1 below shows hydrostatic heads from both study lakes (Doughnut Lake and Goldstream Lake). It appears that flow is alternating between upward flow and downward flow in Doughnut Lake. There appears to be a bifurcation of flow or a fanning of flow. This may indicate the presence of a lateral talik. This may be correlated with a connection to O'Connor Creek to the east of the lake. In Goldstream Lake, the piezometers primarily indicate downward flow, however, it is still very complex. This may be correlated with a deep suprapermfrost talik at the thermokarst margin on the northeast side of the lake and possibly an open talik beneath the lake. This data highlights the complexity of groundwater flow in thermokarst lake systems.

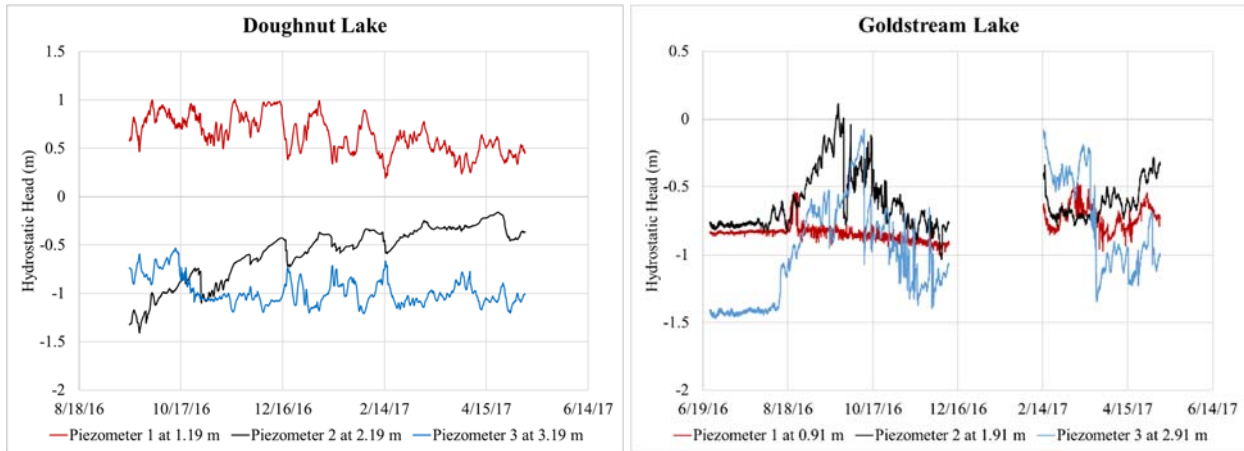


Figure 1. Variation of hydrostatic head with time as reference to the lake water surface in Doughnut Lake (left) and Goldstream Lake (right). Piezometer depths are reported as meters below the sediment-lake interface.

Stable isotope results taken from Goldstream Lake are suggesting that the lake is receiving contributions from subpermafrost or deep groundwater or it receives considerable contributions from degrading permafrost (Figure 2). Doughnut Lake is isotopically different from groundwater due to higher evaporation. However, in April and May of 2016, the isotope values in Doughnut Lake trend towards groundwater, indicating subpermafrost groundwater contributions to the lake. Dissolved ion concentrations indicate that Goldstream Lake may be receiving substantial contributions from degrading permafrost and that Doughnut Lake may have received groundwater contributions in April and May of 2016, but has otherwise been influenced by surface runoff, precipitation, and evaporation. In conclusion, we have determined that advection is a variable and inconsistent CH₄ transport mechanism due to the complexity of flow in these systems.

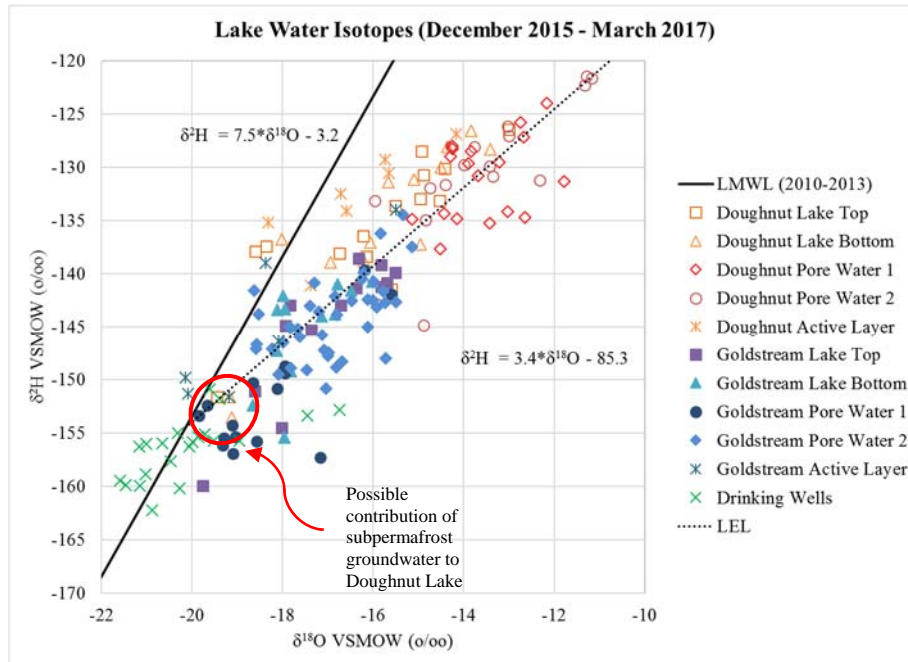


Figure 2. Stable isotopes of deuterium and oxygen-18 sampled monthly from December 2015 to March 2017 are plotted on the Local Meteoric Water Line (LMWL) developed from 2010 to 2013. “Bottom” samples are obtained from the benthic portion of the lake water column. “Top” samples are grab samples obtained from the top of the lake water column. “Pole” samples are obtained from the sediments below the lakes (up to 4 meters below the lake/sediment interface) using Rhizon soil solution samplers that were installed in April of 2016. “Active Layer” samples were obtained from 1” PVC wells installed less than 1 m deep into the active layer around the lake. Black lines intersecting the lake data represent local evaporative lines (LELs) that may be established for each lake system.

Diffusion

Results obtained from analysis of dissolved CH₄ content in the sampling points suggests that diffusion does not contribute greatly to the transport of methane from the subpermafrost environment due to the lack of a consistent concentration gradient (Figure 3). However, large error has been associated with this sampling method requiring analysis of sediment cores. Hammer core samples were obtained in March 2017 and are continuing to be analyzed to further answer these questions.

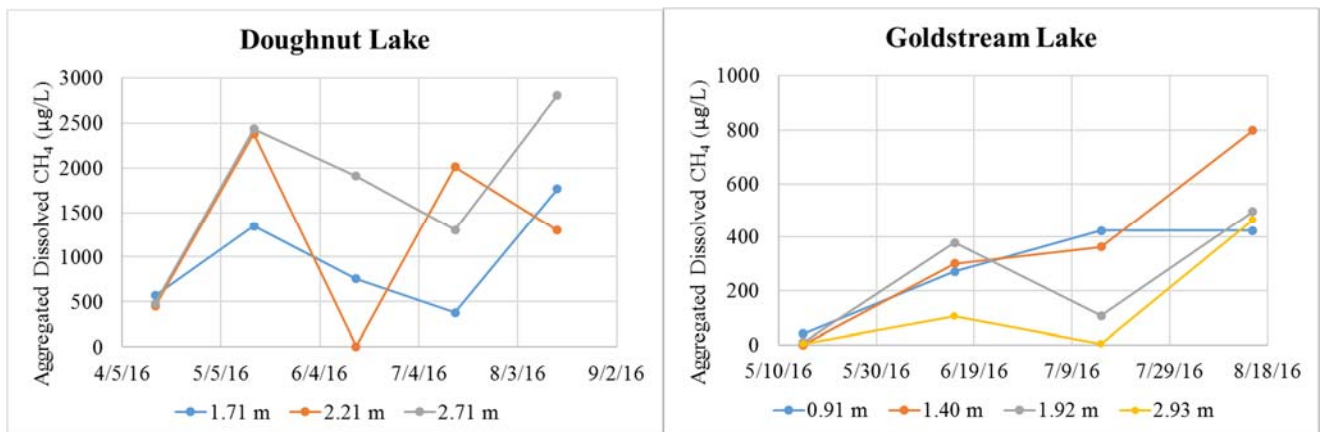


Figure 3. Examples of dissolved CH₄ concentrations in the sub-lake taliks with depth. Depth is reported as meters below the sediment lake interface.

Immiscible Flow

Immiscible flow has been visually observed and recorded. On Goldstream Lake, a sampling point at 2.41 m below the sediment-lake interface serves as a conduit for immiscible flow. With the presence of a silty soil with high organic content, this indicates a displacement pressure of approximately 380 cm of head. We analyzed a representative silt sample from the Fox Permafrost Tunnel using Tempe cells and 5 bar and 15 bar pressure plates. Several soil moisture characteristic curves were developed using the RETC program developed by Genuchten et al. An example of a soil moisture characteristic curve developed using RETC can be seen in Figure 4 that indicates a displacement pressure of 357 cm of head. From observations, immiscible flow appears to be the main CH₄ transport mechanism.

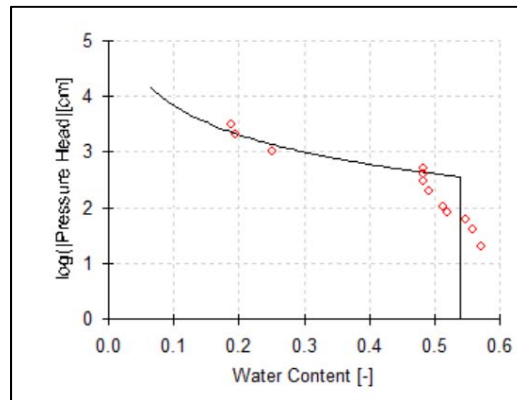


Figure 4. Soil moisture characteristic curve developed for Goldstream silt using a Maulem-Brooks and Corey model in the RETC program.

REFERENCES

- Alberto, M. C. ., Arah, J. R. ., Neue, H. ., Wassmann, R., Lantin, R. ., Aduna, J. ., and Bronson, K. . (2000). "A sampling technique for the determination of dissolved methane in soil solution." *Chemosphere - Global Change Science*, 2(1), 57–63.
- Barnes, M. L. (2014). "Groundwater dynamics in degrading, discontinuous permafrost." University of Alaska Fairbanks. M.S. Thesis.
- Hinkel, K. M., Arp, C. D., Townsend-Small, A., and Frey, K. E. (2016). "Can Deep Groundwater Influx be Detected from the Geochemistry of Thermokarst Lakes in Arctic Alaska?" *Permafrost and Periglacial Processes*.
- Kane, D. L., and Slaughter, C. W. (1973). "Recharge of a central Alaskan lake by subpermafrost groundwater." *The North American Contribution to the Second International Conference on Permafrost, Yakutsk*, 458–462.
- Klute, A. (1986). "Water Retention: Laboratory Methods." *Methods of Soil Analysis, Part 1: Physical and Mineralogical Methods*, Madison.
- Mackay, J. R., and Lavkulich, L. M. (1974). "Ionic and oxygen isotopic fractionation in permafrost growth." *Geological Survey of Canada, Paper 74-1B*, 1, 255–266.

Initiating a network of long-term records of lake-level fluctuations in interior Alaska in relation to climate change

Initiating a network of long-term records of lake-level fluctuations in interior Alaska in relation to climate change

Basic Information

Title:	Initiating a network of long-term records of lake-level fluctuations in interior Alaska in relation to climate change
Project Number:	2016AK131B
Start Date:	3/1/2016
End Date:	2/28/2017
Funding Source:	104B
Congressional District:	AK-001
Research Category:	Climate and Hydrologic Processes
Focus Category:	Geomorphological Processes, Sediments, Ecology
Descriptors:	None
Principal Investigators:	Matthew John Wooller

Publications

1. Bigelow Nancy, Josh Reuther, Matthew Wooller, Emilie Saulnier-Talbot, Kate Mulliken, K., and Katherine Wallace, 2017, Holocene Landscape Change in the Middle Susitna Valley. Poster presented at the Alaska Anthropological Association 44th Annual Meeting. Fairbanks, AK.
2. Fields, Stormy, Matthew Wooller, Nancy Bigelow, Chris Maio, Josh Reuther, Emilie Saulnier-Talbot, 2017, Identifying Diatoms from Lake Sediments in Lost Lake, Alaska. UAF undergraduate research symposium.

Title: Initiating a network of long-term records of lake-level fluctuations in interior Alaska in relation to climate change.

Research summary: This project aimed to develop a network of lake sites in interior Alaska to examine how lake levels have changed in response to long-term environmental changes. Many lakes in interior Alaska are used for recreation and subsistence activities. For example, Quartz, Harding and Birch lakes in interior Alaska (Figure 1) are important sites used for sport fishing and are managed by Alaska Department of Fish and Game which stocks the lakes with fish. However, some lakes in interior Alaska are currently experiencing marked decreases in lake levels. For example, Quartz Lake over the last 10 years has shown a decrease in lake level that has, at times, exposed the large expanses of shallow shelves in the lake. There is an insufficient number of longer-term records of past lake level changes from interior Alaska to determine the extent of regional vs. local trends associated with climate changes. Records that extend beyond the very limited historical data are needed to assess typical lake-level changes and trends for lakes in interior Alaska.

Project objectives included: Conducting diatom analyses of cores that are already available and dated from Quartz and Blair lakes (Figure 1). Use the diatom data generated from Quartz and Blair lakes to develop a quantitative reconstruction of lake level at each site covering the last 10,000 years. Initiate a network and database of multi-millennial, lake-level records for interior Alaska. Compare and contrast lake-level records vs. time for each of these lakes along with previously published records from Grizzly, Harding and Birch lakes (Abbott et al., 2000; Tinner et al., 2015; Finkenbinder et al., 2014) and the lake-level record we have very recently constructed from Lost Lake as part of our previous NIWR project. Compare the lake-level trends in our initiated network relative to long-term (multi-millennial) climate change records for interior Alaska (e.g. Kauffman et al., 2015).



Figure 1: Location of our study sites (Quartz and Blair Lake) and other lakes mentioned in our project and incorporated into a network of long-term, lake-level changes in interior Alaska (Based on a Google map).

Methods and materials: There are two primary methods for reconstructing long-term, lake-level fluctuations using lake sediments and they both come with advantages and disadvantages. The first is considered by some researchers to be the “gold standard” for reconstructing long-

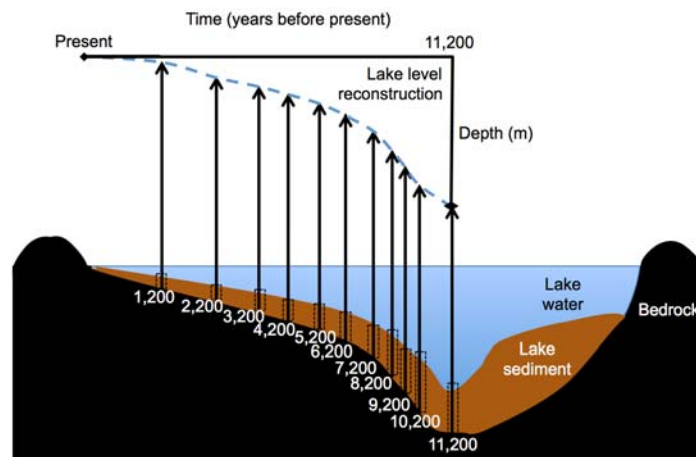
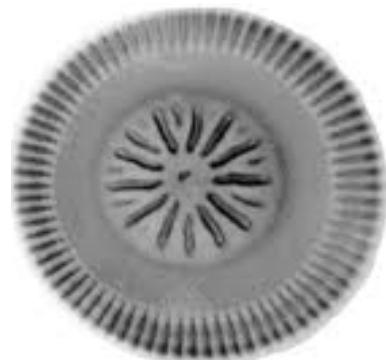


Figure 2: A conceptual figure showing a basic lake-level reconstruction using basal ages of sediment cores taken from a hypothetical lake (Wooller unpublished figure).

term lake-level records. This first approach involves taking a series of sediment cores from a number of locations within a lake and over a depth gradient (e.g., Figure 2). Each core down through these sediments provides a time-line of the lake's history at that location (Figure 2). Evidence of when a lake first appeared and how a lake changed over this time-line is preserved in the layers of mud. When multiple cores are taken on a transect across the lake, going from the deepest part to the edge of a lake, they can be dated and lined up to show how a lake filled over time (Figure 2). By further examining these cores, periods of lake-level decrease can also be identified. This approach has been successfully used to construct coarse temporal resolution records of lake level fluctuations in only two lakes in interior Alaska (e.g., Harding and Birch lakes). This is also the approach we have used to reconstruct lake level changes at Lost lake in interior Alaska. One significant advantage to this approach is that it provides quantitative estimates of the magnitude of lake level changes.

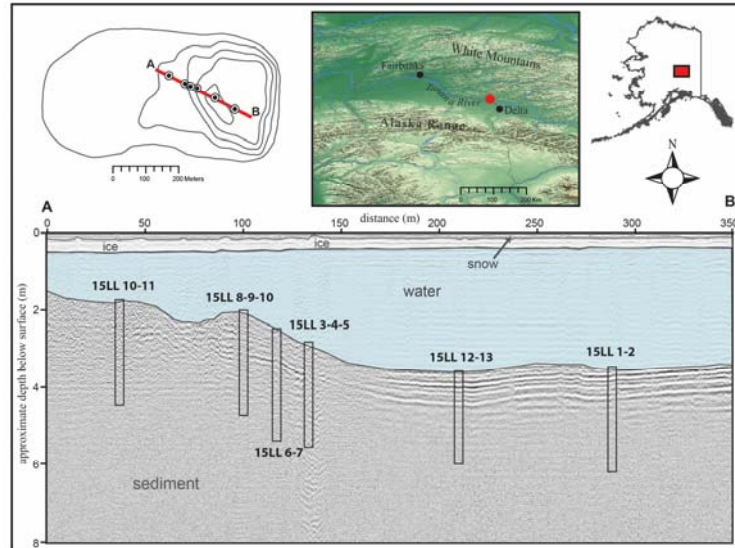
A second approach for reconstructing past lake levels involves focusing attention on analyses of a single, complete sediment core taken from the deepest part of a lake and analyzing evidence preserved in the core that can indicate past lake-level changes. One type of evidence that is particularly valuable for this approach is analyses of diatom remains (silica) preserved in the sediments (Figure 3). Diatoms are microscopic single-celled algae that have a cell wall of silica (called a frustule – Figure 3), which can preserve well over very long periods of time. The characteristic ornamentation of the frustules makes it possible to identify them to the species level. Different species are also favored in shallow lakes compared with deep lakes. Therefore, changes in the diatom assemblages and in their abundance along a dated core can be interpreted qualitatively and also used in a statistical model to infer quantitative changes in past lake depth over time. This approach recently has been successfully applied to Grizzly Lake (Figure 1), in Alaska (Tinner et al., 2015). This approach provides a modeled pattern of lake-level changes over time for a lake. Moreover, there are several considerable advantages to this approach. The first is that it can be conducted on a core taken from a single location in a lake, rather than needing numerous dated cores from one lake. It is considerably more typical for a core to be taken from a single location in a lake and close to the deepest point. This reduces the logistics and costs (i.e. core dating costs) compared to the approach described above. This second approach can also be applied retrospectively to the numerous number of sediment cores taken and already dated from single locations in other lakes. For instance, we have for other, previous projects, taken sediment cores from the deepest locations in Blair and Quartz lakes (Figure 1). These cores have also been radiocarbon dated and have been preserved in cold storage ready for sub-sampling for our diatom analyses, to subsequently compare to the lake-level reconstruction we have created from Lost lake (see

Figure 3: A diatom species (*Discostella pseudostelligera*) (10 microns across) from a core taken from Alaska (photo credit Saulnier-Talbot 2014).



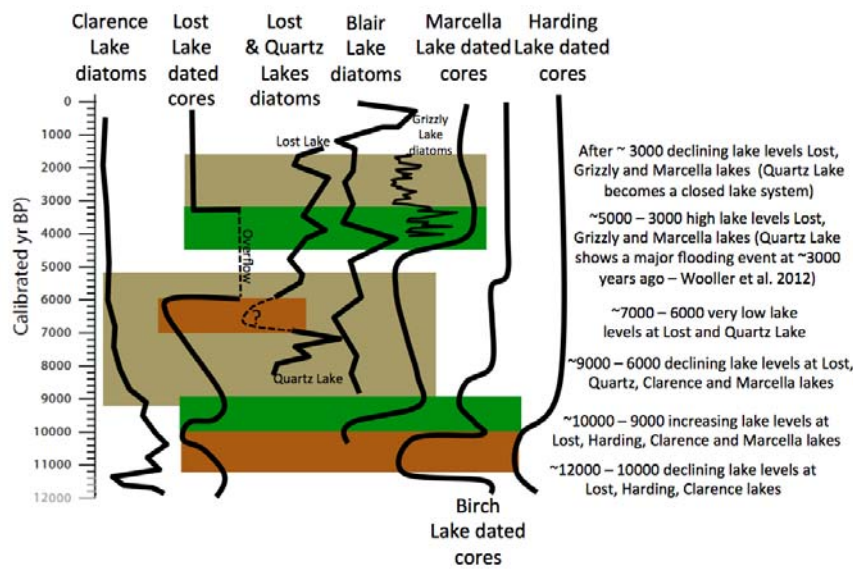
below – Figure 4); other cores are available from other locations as well (i.e., Harding Lake - Finkenbinder et al., 2014 and Birch Lake - Abbott et al., 2000).

Figure 4: Location and ground penetrating radar survey data from Lost Lake, Alaska.



Results and discussion: Records of lake level change were generated from Blair and Quartz Lakes using diatom analyses as part of this project. Diatom analyses were also conducted on the core taken from the deepest location in Lost Lake, to compliment the lake level reconstruction established for the site using radiocarbon dating of multiple cores from across a depth gradient. The survey of multiple cores from Lost Lake also resulted in a ground penetrating radar survey of the lake, which aided the selection of the sites for coring (Figure 4). In the case of Quartz Lake, although samples were prepared and analyzed for diatoms from ~ every 10 cm many of the samples had no diatoms present, which was most likely due to diatoms dissolving during deposition. This resulted in only a very narrow window of time represented by the lake level reconstruction from Quartz Lake (Figure 5). However, because Quartz Lake is adjacent to Lost Lake the two records could be spliced together to provide overall inferences. These two lakes showed several features that were present in both lakes as well as in the sediment core based lake level reconstruction (Figure 5). These included a marked drop in lake levels at ~6,500 years before present and a peak in lake levels at ~4,000 years ago. This peak at ~4,000 years ago also correlated with a feature in the sediment core from Quartz Lake that has previously been interpreted as a major flooding event (Wooller et al. 2012) and also correlated with a peak in lake levels in the previously published records from Blair, Grizzly and Marcella Lakes (Figure 5). Four lakes (Blair, Marcella, Grizzly and Lost Lakes) in our network of lakes all showed a major drop in lake levels after ~3,500 years before present. Four of the lakes in the network (Birch, Lost, Marcella and Harding Lakes) all showed a major increase in lake levels at ~10,000 years before present (Figure 5). The records we generated from Blair, Lost and Quartz Lakes also showed some correspondence with the regional (Alaska) lake level trends compiled in a major

Figure 5: A summary of the lake level records compiled in the lake level network.



review of past climate changes in Alaska (Kauffmann et al. 2016) and with climate change parameters (moisture and temperature) compiled in the same review (Figures 6 and 7).

Figure 6: Lake level changes at Lost and Quartz Lakes plotted relative to lake level trend data summarized in a recent review for Alaska.

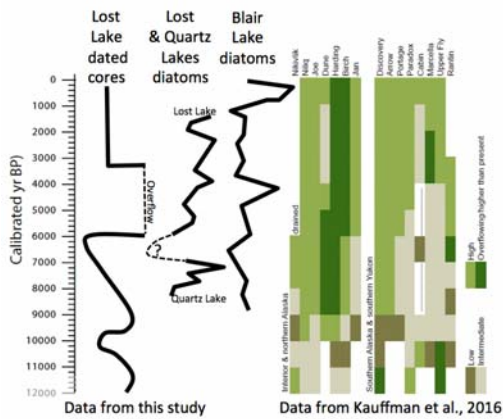
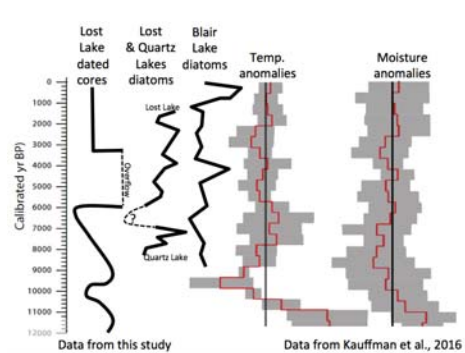


Figure 7: Lake level changes at Lost and Quartz Lakes plotted relative to lake level trend data summarized in a recent review for Alaska.



References:

- Abbott, M, Finney, B, Edwards, M and Kelts, K (2000). Lake-level reconstructions and paleohydrology of Birch Lake, Central Alaska, based on seismic reflection profiles and core transects. *Quaternary Research*. 53: 154-166.
- Anderson, L, Abbott, M, Finney, B, and Edwards, M. (2005). Paleohydrology of the Southwest Yukon Territory, Canada, based on multiproxy analyses of lake sediment cores from a depth transect. *Holocene*. 15: 1172-1183.
- Finkenbinder, M, Abbott, M, Edwards, M, Langdon, C, Steinman, B, Finney, B (2014). A 31,000 year record of paleoenvironmental and lake-level change from Harding Lake, Alaska, USA. *Quaternary Science Reviews* 87: 98-113.
- Kauffmann D. et al., M.J. Wooller (2015). Holocene climate changes in eastern Beringia (NW North America) — A systematic review of multi-proxy evidence. *QSR*. On-Line first.
- Tinner et al., (2015). Late-Holocene climate variability and ecosystem responses in Alaska inferred from high-resolution multiproxy sediment analyses at Grizzly Lake. *Quaternary Science Reviews*. 126: 41-56.
- Wooller, M.J., J. Kurek, B. Gaglioti, L. Cwynar, N. Bigelow, J. Reuther, C. Gelvin-Reymiller, J. Smol. (2012a). An ~11,200 year paleolimnological perspective for emerging archaeological findings at Quartz Lake, Alaska. *Journal of Paleolimnology*. 48: 83-99.

Removal of Toxic Heavy Metals from Contaminated Water Using a Metal-Organic Framework (MOF)-Graphene Oxide (GO) Hybrid Material

Basic Information

Title:	Removal of Toxic Heavy Metals from Contaminated Water Using a Metal-Organic Framework (MOF)-Graphene Oxide (GO) Hybrid Material
Project Number:	2016AK132B
Start Date:	3/1/2016
End Date:	12/22/2017
Funding Source:	104B
Congressional District:	AK-001
Research Category:	Water Quality
Focus Category:	Water Quality, Treatment, Toxic Substances
Descriptors:	None
Principal Investigators:	Lei Zhang

Publication

1. Tonoy Chowdhury, 2017. Removal of Toxic Heavy Metals from Contaminated Water Using a Metal-Organic Framework (MOF)-Graphene Oxide (GO) Hybrid Material Composite (Master thesis, University of Alaska Fairbanks). Three manuscripts are in preparation.

Title: Removal of Toxic Heavy Metals from Contaminated Water Using a Metal-Organic Framework (MOF)-Graphene Oxide (GO) Hybrid Material

Research summary

The nature of the research was primarily laboratory based, with a scope to synthesize MIL-53(Al)-GO nanocomposite and examine its potential as an adsorbent for the removal of As(V), Ni(II), and Pb(II) ions from contaminated water. Major objectives of the proposed research were to:

- (1) *Synthesize MIL-53(Al)-GO and characterize its crystal structure and surface area.*
- (2) *Test the efficacy of MIL-53(Al)-GO for the removal of As(V), Ni(II), and Pb(II) ions and explore the relationship of the adsorption capacity of heavy metal ions as a function of the mass ratio of MIL-53(Al) in MIL-53(Al)-GO.*
- (3) *Develop adsorption isotherm models and measure the kinetics of heavy metal removal on MIL-53(Al)-GO.*

Methods and materials

Materials: Aluminium(III) nitrate nonahydrate ($\text{Al}(\text{NO}_3)_3 \cdot 9\text{H}_2\text{O}$), terephthalic acid (H_2BDC), N,N-dimethylformamide (DMF) were used to prepare MIL-53(Al). Graphene oxide (GO) was synthesized using 99% sulfuric acid (H_2SO_4), graphite, potassium permanganate (KMnO_4) and 30% hydrogen per oxide (H_2O_2). Stock solutions of heavy metals were made by lead(II) nitrate ($\text{Pb}(\text{NO}_3)_2$), nickel(II) nitrate hexahydrate ($\text{Ni}(\text{NO}_3)_2 \cdot 6\text{H}_2\text{O}$), and arsenic ICP standard (10,000 ppm As in 5% HNO_3), respectively. Arsenic ICP standard was purchased from Ricca Chemical Company (Arlington, TX) and the rest of chemicals were purchased from Sigma-Aldrich (St. Louis, MO). Methanol used for washing MIL-53(Al) was purchased from VWR scientific (West Chester, PA). All reagents and solvents were analytic grade and used as received. Deionized water (DI) was produced using a Thermo Scientific Barnstead NANOpure purifying system (18.2 M Ω). Micro porous (4-7 μm) filter papers were used to separate the heavy metal solutions from the adsorbent for atomic spectroscopy analysis.

Synthesis of GO: Graphene oxide was prepared using modified Hummers method (1). 0.5 g graphite powder, 0.5 g NaNO_3 and 23 ml H_2SO_4 (99%) were mixed by stirring in a glass beaker

placed in an ice bath for 4 h. 3 g of KMnO_4 was slowly added to the mixture. The mixture was always kept below $20\text{ }^\circ\text{C}$ to avoid overheating and explosion. After few minutes the ice bath was removed and the temperature of the mixture was increased up to $35\text{ }^\circ\text{C}$ for 1 hour with continuation of stirring. 46 ml of DI water was slowly added to the mixture and temperature was elevated to $95\text{ }^\circ\text{C}$. Aluminum foil was used to cover the beaker to avoid the mixture boiling off. After 2 hours of heating, the mixture was cooled down to room temperature. Then 46 ml of DI water was added and stirred followed by adding 10 ml of 30% H_2O_2 . The reaction mixture was further stirred for about 30 minutes. Finally the brownish product was washed three times with deionized water, centrifuged (8000 rpm, 10 minutes) and freeze dried for 48 hours to obtain GO powder.

Synthesis of MIL-53(Al)-GO nanocomposite with different MIL-53(Al) mass ratios: MIL-53(Al) was synthesized using a method reported in reference (2). 0.788 g of $\text{Al}(\text{NO}_3)_3 \cdot 9\text{H}_2\text{O}$ (2.1 mmol) and 0.518 g of H_2BDC (3.12 mmol) were mixed in 30 ml of DMF. The mixture was put in a 100 ml stainless steel autoclave with a Teflon inset at $130\text{ }^\circ\text{C}$ for 72 hours in an oven. A white gel was obtained and separated by centrifugation (8000 rpm, 10 minutes). The sample was then washed three times with 30 ml methanol and centrifuged as above followed by air dry at $100\text{ }^\circ\text{C}$ overnight. The white product was immersed in methanol (30 ml) for 24 hours, washed and centrifuged three times with methanol following the procedures as above. Finally the sample was dried overnight under vacuum at $110\text{ }^\circ\text{C}$.

MIL-53(Al)-GO nanocomposite was synthesized by dispersing a certain amount of GO powder in 30 ml DMF solution along with $\text{Al}(\text{NO}_3)_3 \cdot 9\text{H}_2\text{O}$ and H_2BDC . The solution was sonicated for 10 minutes to obtain a homogeneous suspension and then subjected to the same synthetic procedure of MIL-53(Al). MIL-53(Al)-GO composite was denoted as n% MIL-53(Al)-GO, where n is the weight percentage of GO used in the reaction mixture, compared with the total weight of the precursors of MIL-53(Al)-GO. For example: 0.013 g GO was used to synthesize 1% MIL-53(Al)-GO, 0.065 g for 5% MIL-53(Al)-GO, and 0.325 g for 25% MIL-53(Al)-GO.

Characterization: The crystal structures of MIL-53(Al)-GO, bare MIL-53(Al), and GO were examined using a PANalytical X'Pert MRD X-ray diffractometer in the Advanced Instrumentation Laboratory (AIL) at the University of Alaska Fairbanks (UAF). A Scientific Nicolet 6700 Fourier Transform Infrared Spectroscopy (FT-IR) at the Chemistry Department

was used to characterize the functional groups in MIL-53(Al)-GO, bare MIL-53(Al), and GO, to determine if MIL-53(Al)-GO was synthesized successfully. A JEOL JXA-8530F Electron Microprobe at the AIL was used to examine the morphologies of MIL-53(Al)-GO, bare MIL-53(Al), and GO. The surface areas of MIL-53(Al)-GO, MIL-53(Al), and GO were measured by nitrogen adsorption at 77 K in the UAF Mechanical Engineering materials laboratory. The samples were degassed at 120 °C for 12 h before measurement. Surface areas were calculated using the Brunauer-Emmett-Teller (BET) model.

Adsorption experiments: Batch experiments of As(V), Ni(II), and Pb(II) adsorption were conducted by mixing known quantities of MIL-53(Al)-GO with different MIL-53(Al) loadings (0.4 to 3 g/L) with As(V), Ni(II), and Pb(II) ion aqueous solutions within a range of 10 to 150 ppm (10 to 450 ppm for Pb) in polyethylene test tubes. Before adsorption, adsorbents were vacuumed to dry at 120 °C for 24 h. The mixture of adsorbent suspension and metal ion solution were well oscillated at room temperature until achieving equilibrium. The solid phase was centrifuged to separate from the solution. Concentrations of As(V), Ni(II), or Pb(II) in the filtrate were determined using an atomic absorption spectroscopy in the Water and Environmental Research Center (WERC) at the UAF.

Adsorption kinetics: 50 ppm of As(V), Ni(II), and 150 ppm of Pb(II) ion solutions was added to the suspension of 0.4 g/L MIL-53(Al)-GO nanocomposites (3% MIL-53(Al)-GO was used for As(V) adsorption and 5% MIL-53(Al)-GO was used for Pb(II) and Ni(II) adsorption). Supernatant was collected at different time intervals and the adsorptive uptake was measured as a function of reaction time until reaching equilibrium. Pseudo-first-order and pseudo-second-order equations were used to explain the diffusion mechanism of heavy metal ions on MIL-53(Al)-GO. The pseudo-first-order equation is defined as:

$$\log(q_e - q_t) = \log q_e - \frac{tk_1}{2.303} \quad (1)$$

where q_e and q_t are the amounts of heavy metal ions adsorbed (mg/g) at equilibrium and at time t (min), respectively, and k_1 (min^{-1}) is the adsorption rate constant. Values of k_1 will be calculated from plots of $\log(q_e - q_t)$ vs. t for the As(V), Ni(II), and Pb(II) adsorption on the sorbents tested. The pseudo-second-order equation is expressed as:

$$\frac{t}{q_t} = \frac{1}{k_2 q_e^2} + \frac{t}{q_e} \quad (2)$$

where k_2 (g/mg min^{-1}) is the rate constant of the pseudo-second-order adsorption, and q_t is the amount of heavy metal ion adsorbed at time t (mg/g). Values of k_2 were calculated from plots of t/q_t vs. t for As(V), Ni(II), and Pb(II) adsorption on the sorbents tested. All experiments were conducted in triplicate.

Results/discussion

(1) Synthesis and characterization of MIL-53(Al)-GO:

X-ray diffraction (XRD) patterns of MIL-53(Al), GO and MIL-53(Al)-GO composites are shown in Figure 1. The characteristic peaks of MIL-53(Al) at 8.8° , 15.25° , 17.75° and 11° for GO confirmed their crystal structures which were in agreement with the previous work (3, 4). MIL-53(Al)-GO composites showed diffraction patterns similar to the pure MIL-53(Al). Interestingly, there was no diffraction peak for GO in the composite as the low content of GO was shielded by the attached MIL-53(Al) particles (5). It was also observed that the crystallinity was reduced when GO content in MIL-53(Al) increased, which is probably due to the MIL-53(Al) cage separation and completely separated GO sheets (6).

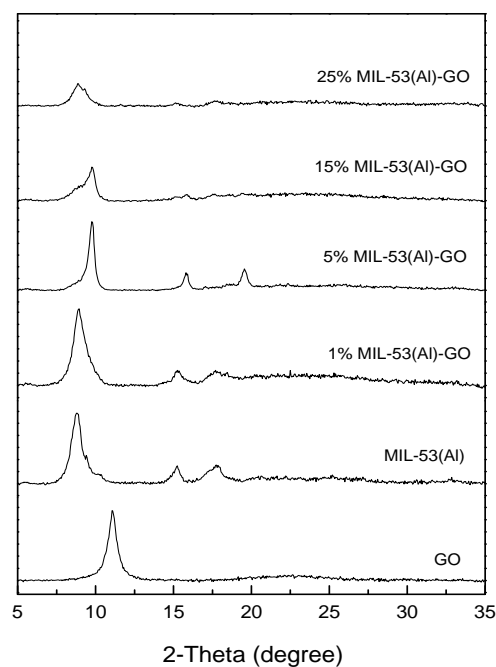


Figure 1. XRD patterns of MIL-53(Al), GO and MIL-53(Al)-GO composites.

In Figure 2, the FT-IR spectra of GO, MIL-53(Al) and composites of them are presented. The spectra of MIL-53(Al) and those of the composites looked rather similar. Characteristic peaks of GO were observed at 3417 cm^{-1} for O–H stretching, 1623 cm^{-1} for C=C stretching, 1722 and 1407 cm^{-1} for carboxyl group stretching and 1230 and 983 cm^{-1} for C–O stretching (4). All of the characteristic peaks were also observed in the spectra of MIL-53(Al) and its composites. Apart from this, MIL-53(Al) and MIL-53(Al)-GO composites showed other peaks associated with benzene ring in terephthalic acid ligand (C–H at 1095 cm^{-1}) and –OH stretching at around 3500 cm^{-1} .

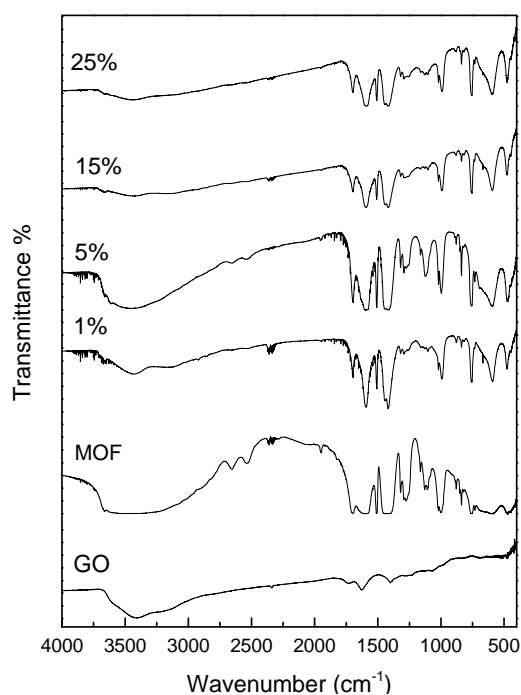


Figure 2. FTIR spectra of MIL-53(Al), GO and MIL-53(Al)-GO composites with different weight percentage of GO added (1%-25%).

BET surface areas of MIL-53(Al), GO and MIL-53(Al)-GO composites are listed in Table 1. It showed that surface areas of composites increased as the ratio of GO increased. Additional porosity of MIL-53(Al)-GO composites developed might be the reason of (a) separation of cages of MIL-53(Al) due to the intersection of GO layers and (b) attachment of epoxy and hydroxyl functional groups of GO layers with MIL-53(Al) (6). The highest surface area was recorded for

2% MIL-53(Al)-GO, which is around 18% and 500% higher than pure MIL-53(Al) and GO, respectively. A reduction in surface area is observed when the weight percent of GO added is higher than 3%. A high content of GO was not suitable for composite formation due to the limited capability of the GO sheets to attach with MIL-53(Al) in some orientations. That's why an MIL-53(Al)-GO composite with low content of GO showed higher surface area.

Table 1. BET surface area of GO, MIL-53(Al) and MIL-53(Al)-GO composites.

Adsorbent	BET Surface Area (m ² /g)
GO	213
MIL-53(Al)	1079
1% MIL-53(Al)-GO	1154
2% MIL-53(Al)-GO	1273
3% MIL-53(Al)-GO	1147
5% MIL-53(Al)-GO	1050
10% MIL-53(Al)-GO	817
15% MIL-53(Al)-GO	775
25% MIL-53(Al)-GO	365

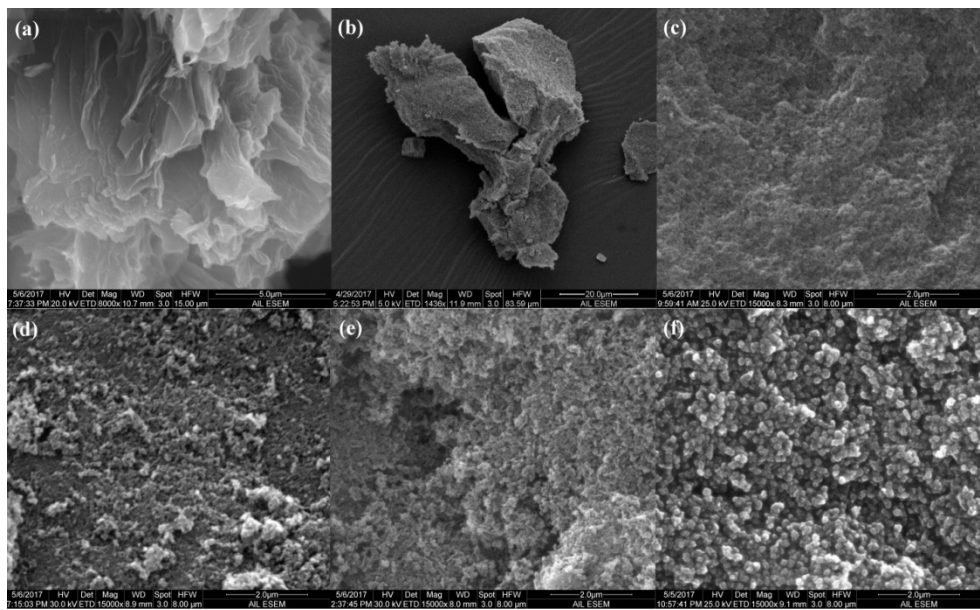


Figure 3. SEM images of (a) GO, (b) MIL-53(Al), (c) surface of MIL-53(Al), (d) 5% MIL-53(Al)-GO (e) 15% MIL-53(Al)-GO and (f) 25% MIL-53(Al)-GO.

SEM images of the materials are shown in Figure 3, which show the morphology of GO, MIL-53(Al) and MIL-53(Al)-GO composites.

(2) Test the efficacy of MIL-53(Al)-GO for the removal of As(V), Ni(II), and Pb(II) ions and explore the relationship of the adsorption capacity of heavy metal ions as a function of the mass ratio of MIL-53(Al) in MIL-53(Al)-GO.

Table 2. Adsorption of As(V), Ni(II), and Pb(II) ions with GO, MIL-53(Al) and MIL-53(Al)-GO composites (10 mg of adsorbent in 25 mL 100 ppm metal solution for 24 hours).

Adsorbent	q_e for As (mg/g) ^a	q_e for Ni(II) (mg/g) ^a	q_e for Pb(II) (mg/g) ^a
GO	5.98	14.18	141.48
MIL-53(Al)	32.65	2.1	127.61
1% MIL-53(Al)-GO	49.73	22.65	179.6
2% MIL-53(Al)-GO	51.43	24.375	183.6
3% MIL-53(Al)-GO	51.80	22.3125	154.0
5% MIL-53(Al)-GO	44.45	29.575	205.4
10% MIL-53(Al)-GO	43.53	14.2	151.3
15% MIL-53(Al)-GO	32.45	27.575	133.1
25% MIL-53(Al)-GO	37.55	15.8375	44.7

^a q_e is the equilibrium adsorption capacity of heavy metal ions in the specimen.

The equilibrium adsorption capacities of GO, MIL-53(Al) and MIL-53(Al)-GO composites are shown in Table 2. It is clear that the adsorption of heavy metal ions tested increased as the GO content in the MIL-53(Al) increased but up to a certain level. As(V) ion adsorption was found to be the maximum in 3% MIL-53(Al)-GO composite, and it was 58% and 766% higher than that in MIL-53(Al) and GO, respectively. In contrast, 5% MIL-53(Al)-GO composite exhibited the maximum adsorptions of Ni(II) and Pb(II) ions, which were 1308% and 61% higher than MIL-53(Al) and 61% and 45% higher than GO, respectively. Adsorption is primarily dependent on the porosity of an adsorbent. In our study, the maximum surface area was found for 2% MIL-53(Al)-GO composite, while the maximum heavy metal adsorption was obtained in 3% and 5% MIL-53(Al)-GO composites. Similar results have been reported in previous works on MOF-GO composites (6). We assume that, the pore diameters of 3% and 5% MIL-53(Al)-GO composites were suitable (smaller than the molecular size of As(V), Ni(II) and Pb(II) ions) for heavy metal adsorption though further research is required to establish our assumption.

(3) Develop adsorption isotherm models and measure the kinetics of heavy metal removal on MIL-53(Al)-GO.

The adsorption data were analyzed according to the Langmuir adsorption isotherm model (Equations (3)), which assumed that adsorption takes place at specific homogeneous sites within the adsorbent.

$$\frac{C_e}{q_e} = \frac{C_e}{q_{\max}} + \frac{1}{q_{\max}K_L} \quad (3)$$

where, C_e is the equilibrium concentration of the heavy metal ions (mg/L), q_e and q_{\max} are the equilibrium adsorption capacity and the maximum adsorption capacity (mg/g), respectively, K_L is the Langmuir constant (L/mg). Parameters of Langmuir isotherm for As(V), Ni(II) and Pb(II) adsorption are listed in Table 3. The high values of R^2 of Langmuir model indicate that the adsorption of all the heavy metal ions fit well with the Langmuir model, and the adsorptions were directed by monolayer adsorption on a homogenous surface. Langmuir isotherms for the As(V), Ni(II) and Pb(II) adsorption are shown in Figure 4a-c. The maximum adsorption capacities (q_{\max}) of composites were much higher than that of the pure MIL-53(Al) and GO.

A very fast kinetics was observed for all the three heavy metal ions tested. The effect of time on As(V), Ni(II) and Pb(II) ions adsorption is presented in Figure 4d-f. The equilibrium adsorption time was 60, 30 and 180 minutes for As(V), Ni(II) and Pb(II) ions, respectively. The kinetics data were analyzed using pseudo first and second order models (equations 1 and 2), and it was found that all the heavy metal ions adsorption fit best with the pseudo second order model.

Table 3. Langmuir isotherm parameters for As(V), Ni(II) and Pb(II) adsorption in GO, MIL-53(Al), and MIL-53(Al)-GO composites.

Heavy Metal	Temperature (K)	Adsorbent	Langmuir Parameters		
			q_{\max} (mg/g)	K_L (L/mg)	R^2
As(V)	296	GO	2.80	0.05	0.970
		MIL-53(Al)	53.19	0.06	0.981
		3% MIL-53(Al)-GO	64.97	0.24	0.999
Ni(II)	296	GO	2.86	0.09	0.929
		MIL-53(Al)	3.05	0.29	0.997

		5% MIL-53(Al)-GO	41.39	0.03	0.971
Pb(II)	296	GO	170.35	0.12	0.993
		MIL-53(Al)	154.79	0.10	0.998
		5% MIL-53(Al)-GO	221.72	0.43	0.996

Figure 4. Langmuir isotherms of (a) As(V) adsorption in 3%MIL-53(Al)-GO, (b) Ni(II) adsorption in 5%MIL-53(Al)-GO, and (c) Pb(II) adsorption in 5%MIL-53(Al)-GO; the effect of time on (d) As(V), (e) Ni(II) and (f) Pb(II) ions adsorption in GO, MIL-53(Al), and MIL-53(Al)-GO composites.

References

1. Dey, R.S., Hajra, S., Sahu, R.K., Raj, C.R., Panigrahi, M.K. 2012, A rapid room temperature chemical route for the synthesis of graphene: metal-mediated reduction of graphene oxide, *Chem Commun.*, 48(12), 1787-1789.
2. Ricco, R., Konstas, K., Styles, M.J., Richardson, J.J., Babarao, R., Suzuki, K., Scopce, P., Falcaro, 2015, P. Lead(ii) uptake by aluminium based magnetic framework composites (MFCs) in water, *J Mater Chem A.*, 3(39), 19822-19831.
3. Tien-Binh, N., Vinh-Thang, H., Chen, X.Y., Rodrigue, D., Kaliaguine, S. 2015, Polymer functionalization to enhance interface quality of mixed matrix membranes for high CO₂/CH₄ gas separation, *J Mater Chem A.*, 3(29), 15202-15213.
4. Kyzas, G.Z., Deliyanni, E.A., Matis, K.A. 2014, Graphene oxide and its application as an adsorbent for wastewater treatment, *Journal of Chemical Technology & Biotechnology*, 89(2), 196-205.
5. Wu, Z., Yuan, X., Zhong, H., Wang, H., Zeng, G., Chen, X., Wang, H., Zhang, L., & Shao, J. 2016, Enhanced adsorptive removal of p-nitrophenol from water by aluminum metal-organic framework/reduced graphene oxide composite, *Scientific Reports*, 6, 25638.
6. Ahmed, I., Jhung, S.H. 2016, Remarkable adsorptive removal of nitrogen-containing compounds from a model fuel by a graphene oxide/MIL-101 composite through a combined effect of improved porosity and hydrogen bonding, *J Hazard Mater.*, 314, 318-325.

Variable lapse rates and the mass balance of a well-studied glacier in south-central Alaska

Basic Information

Title:	Variable lapse rates and the mass balance of a well-studied glacier in south-central Alaska
Project Number:	2016AK133B
Start Date:	3/1/2016
End Date:	2/28/2017
Funding Source:	104B
Congressional District:	AK-001
Research Category:	Climate and Hydrologic Processes
Focus Category:	Water Quantity, Water Supply, Climatological Processes
Descriptors:	None
Principal Investigators:	Roman Dial, Jason Geck

Publication

1. Data collected here will be presented at the 7th International Polar and Alpine Microbiology Conference in Greenland during September. We have made no public presentations to date but intend to use this report as the basis of a paper to be submitted to Journal of Glaciology or The Cryosphere.

Title: Variable lapse rates and the mass balance of a well-studied glacier in south-central Alaska

Research Summary

Abstract Spatially distributed models of discharge from snowmelt rely on lapse rates -- the algebraic relationship between elevation and temperature -- to extend point data observations of temperature across their modeled landscapes. Lapse rates are often assumed constant, or if variable, to be continuously negative during the melt season. Inverted lapse rates (inversions) reflect increasing temperature over elevation and are generally assumed absent. We show here frequent, persistent, and deep temperature inversions in the accumulation zone of the well-studied Eklutna and nearby Whiteout glaciers in southcentral Alaska over 200 m elevation (1,376 – 1,583 m asl). In addition, we document inverted daily melt rates between 1,376 – 1,505 m asl in the Eklutna's upper basin. Melt rate inversions were less extreme than temperature inversions, but generally led to indistinguishable daily melt rates across 129 m of elevation during 15 May -- 19 July, 2016. Together these results suggest that distributed models that apply lapse as a model parameter that is always negative may underestimate snowmelt and over-estimate mass balance.

Objectives

Models of snowmelt, useful in hydrologic studies forecasting water availability, are of two general types, physical and phenomenological. Physical models begin from first principles and take an energy balance approach. Phenomenological models apply an index approach, typically using air temperature which tends to be well correlated with energy balance. Spatially distributed degree-day models calculate melt across ice and snow-covered landscapes. They require explicit spatial information about topography as found in a digital elevation model (DEM), and generally one or more point measures of temperature. Then, using a “lapse rate” – the relationship between temperature and elevation -- with solar irradiance, DEM-derived slope, and aspect, sub-models apply heat balance equations to snow and ice melt. Such models as Hock (2003) and WaSim (Schulla and Jasper 2007) are useful in hydrological predictions of discharge due to spring runoff in watersheds or seasonal melt in glacierized basins. However, the models, even physical process models (Beamer et al. 2016) can be no better than their parametrizations.

Generally, air temperatures cool with a rise in elevation both above ground and above sea level. A lapse rate describes the algebraic relationship between temperature decrease and elevation increase. “Adiabatic lapse” is the cooling rate of rising air. It can be theoretically derived from the first law of thermodynamics and the relationship between pressure and elevation as $L_A = -9.8^\circ\text{C km}^{-1}$. “Environmental lapse” is the gradient in temperature over elevation in a fixed atmosphere. While it varies substantially in time and space (Minder et. al, 2010), most studies in hydrology, glaciology, and ecology consider it a constant, $L_E = -6.5^\circ\text{C km}^{-1}$, sometimes called the “wet adiabatic lapse”. This assumption of a constant L_E is rare in atmospheric science because it is precisely the variability in L_E that leads to atmospheric instability, such as the generation of thunderclouds and tornadoes. Local weather conditions, surface albedo, and other conditions can lead to $|L_E| > |L_A|$, where the environmental lapse is steeper than the adiabatic lapse. This condition means that a rising parcel of air cannot cool sufficiently quickly to match the cooler air around it, which would otherwise stop its rise. Instead, the air continues to rise as

high as 10 km, dragging air and moisture along with it. Generally, environmental lapse rates in maritime or coastal climates are less steep than continental climates, hence the rarity of coastal thunderstorms and their high frequency in interior climates.

The most extreme example of variable lapse rates are temperature inversions. Under inverted conditions an increase in elevation brings about a *warming* of air temperature. The lapse rate is not negative, but rather positive, $L_E > 0$. Temperature inversions are common in still, winter air, especially under clear skies at high latitudes because the net radiation from the earth is negative. The Earth is losing heat faster than it is gaining it. A second type of inversion occurs when a warmer, less-dense air mass advects over a cooler, denser air mass. These conditions may be common in the mountains of Alaska along the Gulf of Alaska. There oceanic currents from the south deliver heat to the Gulf that then warms the air above it. This air passes across cold glaciers in the coastal ranges with the potential to drive inversions there.

The Eklutna watershed in southcentral Alaska, about 40 km NE of the Prince William Sound of the Gulf of Alaska and 40 km E of Anchorage provides both water and electricity to the State's largest population center. Since 2008 Alaska Pacific University (APU) has conducted hydrologic studies in Eklutna's glacial watershed. Currently, Johnse Ostman using WasSim (Schulla and Jasper 2007) and Jason Geck using the Hock model (Hock 2003) are applying distributed models that rely on lapse rates. Their current implementations use constant lapse rates both in time and space. However, melt-rates from a similarly situated glacier on the Kenai Peninsula suggests that summer-time inversions are common.

Here we report results of the 2016 melt-season study on lapse rates on the Eklutna and its neighbor the Whiteout Glacier. We set out two temperature stations on the Whiteout, five on the Eklutna and one at the pass in between, for a total of eight. We also set out three cameras to record ablation rate and three anemometers to investigate wind speed and direction. Our goal was to establish the role and cause of temperature inversions in mass balance. A secondary goal was to include both undergraduates and masters students in the research. We met these goals through the following objectives:

1. *Document the frequency, extent, timing and depth of melt-season temperature inversions in the accumulation zones of the Eklutna and Whiteout Glacier.*
2. *Document the frequency, extent, timing and depth of melt-season melt-rate inversions in the accumulation zones of the Eklutna and Whiteout Glacier.*
3. *Investigate meteorological correlates with these inversions.*
4. *Include APU students in the data collection and analysis.*

Methods

Study Site The Eklutna Glacier (29.5 km²) is a well-studied (Sass et al., 2009, Larquier et al. 2010, Sass 2011, Loso 2011, 2013, McGrath et al. 2015, Sass et al., 2015, Sass et al. 2017) glacier in southcentral Alaska. The Whiteout Glacier (35.8 km²) is immediately south of and contiguous with Eklutna (Fig. 1). The Eklutna has been visited by APU students near-annually since 2007 to collect mass balance measures, often during a three-week field course entitled "Field Glaciology and Glacier Travel". Eklutna Glacier provides up to 90% of the municipal water each year and 10-20% of municipal electricity. Four APU students, three graduate students and two undergraduates (including a female) were involved in field and labwork described here.

Field-work Using help from graduate students with projects requiring these data and undergraduates gaining experience in STEM, we established eight stations across two glaciers to monitor temperatures over the melt season. Four of these stations also monitored melt and four measured wind speed and direction. Sensors were deployed in two trips in May 2016 and all recorded temperatures 15 May 15 to 11 September, 2016. Table 1 and Fig. 1 give locations and data recorded on the date of deployment.

One field trip used helicopter access with foot travel as a means of retreat; all others used helicopter access into and off the glaciers. Tripods constructed from materials purchased locally with our own design were assembled from one-inch conduit and “floated” on the glacier surface. Temperature sensors were installed at 2 m above the surface at all stations (Table 1). Anemometers attached to cross pieces on three tripods were oriented north when installed. Subsequent melt rotated the tripods at Whiteout.Mid, EKL.Acc1 and EKL.Acc2 rendering wind velocity data there suspect (wind speed available); only ELA.2016 offered wind velocity. At three locations (Ablation, EKL.mid, and EKL.Acc.1) we installed ablation stakes marked with electrical tape at 10 cm intervals. These stakes were photographed using interval photography taken every six hours with waterproof cameras installed on the tripods near to but with ablation stakes in view. Dataloggers recorded the wind and temperature data. A more fully outfitted automated weather station (AWS) at ELA.2016 also recorded relative humidity, broadband albedo, and precipitation, as well as snow surface lowering using a sonic ranging sensor. All data at all stations were logged as hourly means. Wind direction was not logged at the ELA.2016 AWS until 15 June; wind data from non-ELA stations are not presented in this report. Tripod movement restricted the photographic evidence of melt rate so that only melt rates from 15 May to 28 July for ELA.2016, EKL.mid, and EKL.Acc2 are presented.

Analysis Statistics were performed in R (vers. 3.4.0). Lapse rate was calculated hourly because distributed models such as Hock calculate at hourly intervals and data were recorded at the same hourly times across stations. In a preliminary analysis, we regressed the temperatures collected from all 8 stations at a given time t against the elevations of the stations recorded during sensor installation (Table 1). Each hour from midnight 15 May to 1100 hours 11 September generated a value for lapse rate through simple linear regression of temperature (at hour h , T_h) on elevation in meters (E), as $T_h = b_o + b_l E$. Lapse rate was defined as $1000 b_l$, so that units were $^{\circ}\text{C km}^{-1}$. Lapse is considered inverted if the slope, b_l , is positive. The lapse value assumed in the literature is $L_E = -6.5^{\circ}\text{C km}^{-1}$. These values and all other meteorological values (except wind direction) were averaged over day of year as daily means.

Preliminary analysis showed the Ablation station was generally an outlier along the regression line of upper elevations. Our interest is the “anomalous” Eklutna upper basin mass loss (Sass 2011), so we restricted our analysis of inverted lapse rates to elevations above 1,375 m asl. If lapse rates are often inverted above the equilibrium line altitude (ELA), then distributed melt models applying negative lapse rates will underestimate melt in the accumulation zone and so overestimate mass balance.

Degree-day models of melt rate over a time interval (w , in e.g., w.e. cm d^{-1}) take their simplest form as $w = f dds$, where dds is the sum of thawing-degree days across n days of a time interval,

$$dds = \sum_{d=1}^n T^+$$

with $T^+ = \text{mean daily measured air temperature, } T$, if $T > 0^\circ\text{C}$ and $T^+ = 0$ otherwise. The constant f , called the “degree day factor”, is found by regressing melt rate against dds . In this report, we do not convert measured surface lowering to water equivalents. “Melt rate” here is measured surface lowering of the snow in cm d^{-1} . The standard glaciological approach assumes that a snow density profile is similar across sites located within a given mass balance zone (i.e., ablation, accumulation, ELA), so our approach may be a reasonable first approximation if we assume the snow density profiles are similar at ELA.2016, ELK.Mid and EKL.Acc2. Future treatment of these data will use snow-pit data from the ELA.2016 and EKL.Acc2 stations.

Table 1. Weather stations on the Whiteout and Eklutna Glaciers.

Station	Melt	Wind	GNSS Height (m asl)	Latitude	Longitude
Ablation	X		1148.176	61.24211602	-148.9849732
ELA.2016	X	X ^v	1376.288	61.2115636	-148.9575564
EKL.mid	X		1449.204	61.19563419	-148.9548241
Whiteout.Mid		X ^s	1452.491	61.17770487	-148.9045656
EKL.Acc2	X	X ^s	1504.563	61.19638706	-148.9333888
Whiteout.Acc			1513.607	61.18394492	-148.9290434
EKL.Acc1		X ^s	1517.26	61.18182347	-148.9651947
Crest			1583.521	61.1898757	-148.9307926

X = collected; s = wind speed; v = wind velocity

Results

We first document the existence, strength, and timing of inverted lapse rates across the Eklutna and Whiteout Glaciers and inspect point-location measures of standard meteorological measurements at ELA.2016 to infer potential correlations. Next we show that melt, too, can be inverted. Finally, we show variation in the response of melt-rate to degree-day sum across elevations.

Lapse rates over time Lapse rates in the upper basins of Eklutna and Whiteout Glaciers were highly variable, mostly inverted, and rarely at or below $L_E = -6.5^\circ\text{C km}^{-1}$ (Fig. 2). When averaged daily, the mean daily lapse rate ($\bar{L} = +5.4^\circ\text{C km}^{-1}$) minus its standard deviation ($\text{sd} = 10.39^\circ\text{C km}^{-1}$) surpassed L_E ($\bar{L} - \text{sd} = -4.97^\circ\text{C km}^{-1} > -6.5^\circ\text{C km}^{-1}$).

Three periods during the melt season were very strongly inverted: a few days in mid-June, ten days in mid-July, and a week in late August and early September (Fig. 2, pink color between vertical gray bars). As an indication of the strength of these inversions and as evidence that the

very high lapse values are not a statistical artifact, we plotted hourly temperature by elevation for each of the seven upper basin stations (Fig. 3). The coefficients of determination (R^2) in Fig. 2 were generally high (median[R^2] = 0.67, max[R^2] = 0.94) with both strongest inversion (30-40 °C km⁻¹) and highest R^2 (> 0.8) occurring 17-18 July (DOY = 199-200) during the ~12 hours before the inversion broke.

Lapse rates and weather Inspection of standard meteorological variables (“SMV”: temperature, T, relative humidity, RH, albedo, A, wind speed, WS) from the ELA.2016 station (Figs. 4-5) over the three time periods of very strong inversions showed no obvious pattern. Notably, periods of very strong inversions (indicated in Figs. 2, 4-5 by vertical gray lines) occurred at high, moderate, and low wind speeds (Fig. 5a, c-d). Wind direction in late August and early September period is unknown, since a southerly direction was generally indicated in the resting position of the anemometer with wind speed < 5 m s⁻¹.

Pairwise correlations among hourly SMV and lapse were all weak ($|r| < 0.23$) with strongest lapse correlates RH (-0.13) and WS (0.11) similar to strongest daily ($|r| < 0.28$) lapse correlates: RH (-0.20) and WS (0.10). A backward stepping multiple linear regression beginning with all interactions and ending with all interactions significant ($p < 0.05$) suggested that hourly lapse rate covaried negatively with each SMV; positively with all pairwise interactions between SMV; and negatively with the three-way interaction T:RH:A. However, overall fit was poor ($R^2 = 0.06$), strongly suggesting that larger temporal scale processes were responsible. A similar pattern emerged for daily lapse ($R^2 = 0.14$): all SMV coefficients were negative; pairwise interaction coefficients were positive; and the three-way interaction (T:RH:A) coefficient was negative. The main difference between hourly and daily models was that all pairwise interactions with T and RH were present, but not albedo or wind speed. Overall these results suggest a complicated but weak relationship between lapse and weather, with increasing T, RH, A and WS all tending to weaken inversions, their interactions tending to strengthen them, and the difficult to interpret three-way interaction T:RH:A weakening inversions.

Melt inversions Melt inversions were observed in the upper Eklutna basin from 15 May – 28 July as negative differences between daily melt at lower and upper elevations (Fig. 6). Nearly half of all 75 days when melt was measured showed melt inversions within the Eklutna Basin (Table 2). Day-by-day inversions in melt did not clearly match day-by-day inversions in temperatures (Fig. 2). The very-strong, two-day temperature inversion in mid-June roughly matched a strong inversion in melt between ELA.2016 and EKL.Mid stations, but not between EKL.Mid and EKL.Acc2. Similarly, the very strong 10-day inversion mid-July corresponded with melt inversions between EKL.Mid and EKL.Acc2, but not between ELA.2016 and EKL.Mid stations. When melt differences were averaged across 15 May – 28 July, the mean values were near zero (Table 2). This suggests that there was little overall difference in melt despite elevation differences, with little difference between the highest and lowest elevation stations sampled even though separated by 129 m of elevation. When averaged across days the mean \pm se difference included zero for all three combinations consistent with a lack of statistically significant differences between any two (Table 2).

Table 2. Differences in melt between Eklutna basin stations.

Paired melt (n = 75 days)	Difference in elevation (m)	Percent of melt inversion days	Mean difference in melt (cm d ⁻¹)	Standard error melt difference (cm d ⁻¹)	Paired-samples t-test p-value
ELA.2016 and EKL.Mid	56	45%	-0.01 (inverted)	0.31	0.98
EKL.Mid and EKL.Acc2	73	44%	0.28	0.38	0.98
ELA.2016 and EKL.Acc2	129	48%	0.27	0.35	0.44

Degree-day models The two highest stations EKL.Acc2 and EKL.Mid showed nearly identical cumulative degree-day sums, reflecting the frequent inversions there. The degree day sums at the higher elevation stations were considerably higher than at the lower elevation ELA.2016 station (Fig. 7a). The ELA.2016 *dds* lagged the higher elevation stations by almost 10 days at the end of the period. Cumulative melt was less inverted overall than degree-day sum (Fig. 7b), although until mid-July, cumulative melt at the EKL.Mid station, located 73 m above the ELA.2016 station, was greatest. Cumulative melt at the highest station, EKL.Acc2, was less than the other two, but the gap narrowed as time progressed, suggesting the inversion in temperatures allowed it to “catch-up”. Cumulative melt was substantially highest at EKL.Mid until mid-June, indicating a strong melt inversion.

Applying a degree-day model approach (Fig. 7c) suggested that overall the degree-day factors of the two highest stations were equal (parallel slopes); however, degree-day factor at the lowest station was roughly 50% steeper, possibly due to red-snow algae reducing albedo there. Supporting that speculation and drawing attention to the temperature inversion is that at the 0.25 m cumulative melt mark, EKL.Mid was two days ahead of ELA.2016; at 0.5 m melt, it was four days ahead; and at 1 m one week ahead, evidence that temperature inversions in the upper basin of Eklutna are reflected in melt inversions (Fig. 7d).

Discussion

This study documents frequent, deep, and persistent temperature inversions in the accumulation zone of a well-studied Alaskan Glacier. Moreover, these temperature inversions are reflected in inversions in melt rates. Melt rate inversions were not as marked as temperature inversions, possibly due to albedo effects of algae at lower elevations, but revealed themselves as no significant difference in melt measured over 75 melt-season days at stations up to 129 m vertically apart. Most distributed melt models apply a constant lapse of $L_E = -6.5^\circ\text{C km}^{-1}$, which if applied to a difference in elevation of 129 m = 0.129 km suggests a temperature difference of 0.84°C, or nearly one additional degree-day each day, which would suggest a difference in melt equal to number of days multiplied by the degree-day factor.

Because the inversion effect we document here is in the accumulation zone of the Eklutna and Whiteout Glaciers, it likely leads to greater mass wastage than expected, because each year’s additional accumulation would be less than predicted. Melt-season temperature inversions may be responsible, at least in part, for anomalous thinning seen in the Eklutna basin since 1950

(Sass, 2011) and on the Harding Icefield (VanLooy et al., 1998), the latter a much bigger glacier with more discharge, where melt and temperature inversions have been noted (Ganey, 2015).

A regional study of discharge in the Gulf of Alaska drainage basin (Beamer, et al. 2016) compared modeled loss to that observed using Gravity Recovery and Climate Experiment (GRACE) and airborne altimetry data. The dominant discharge term in their favored model was snowmelt, a term likely sensitive to model lapse values. In general, most simulations of Beamer, et al. (2016) found less discharge than observed with GRACE, noting an overall underestimate of 19% averaged over 2004-2013. Lapse rates used in their models varied from -8.2 to $-4.4^{\circ}\text{C km}^{-1}$ with no melt season inversions.

We are in the process of collecting more data this season to further validate the effect and investigate potential causes. We anticipate a peer-reviewed submission that will include another year's data and air movement data from Hysplit simulations. Future instrumentation would best include melt measures at each temperature station, additional albedo measures, and stabilized wind measurements.

References

Beamer, J. P., et al. (2016) "High-resolution modeling of coastal freshwater discharge and glacier mass balance in the Gulf of Alaska watershed." *Water Resources Research* 52.5, 3888-3909.

Ganey, G.Q. 2015. *The role of red snow algae in snowmelt and their nutrient limitation*. MS Thesis. Alaska Pacific University

Hock, R. (2003) Temperature index melt modelling in mountain areas. *J. Hydrol.* 282, 104-111.

Larquier, A. M., Loso, M., & Sass, L. (2010, October). Glacial influences on water resources of the Eklutna basin, Alaska. In *2010 GSA Denver Annual Meeting*.

Loso, M. (2011), The diminishing role of glacier runoff into Eklutna Lake: Potential impacts on hydropower and water supply for the Municipality of Anchorage, Final Rep. Natl. Inst. Water Resour. 2010AK87B, NIWR Funded Res. Proj., Alaska Pac. Univ., Anchorage, Alaska.

Loso, M. (2013) Eklutna Glacier: Mass balance, fluvial discharge, and implications for downstream users. Five year report. Report to Municipal Light and Power, Anchorage, AK.

McGrath, D., Sass, L., O'Neel, S., Arendt, A., Wolken, G., Gusmeroli, A., ... & McNeil, C. (2015). End-of-winter snow depth variability on glaciers in Alaska. *Journal of Geophysical Research: Earth Surface*, 120(8), 1530-1550.

Minder, J. R., Mote, P. W., & Lundquist, J. D. (2010). Surface temperature lapse rates over complex terrain: Lessons from the Cascade Mountains. *Journal of Geophysical Research: Atmospheres*, 115(D14).

Sass, L., M. G. Loso, and J. Geck. "Point measurements of surface mass balance, Eklutna Glacier, Alaska, 2008-2015." (2017). <https://doi.org/10.5066/F7MP51CB>

Sass, L. C., Loso, M. G., Geck, J., Thoms, E. E., & Mcgrath, D. (2017). Geometry, mass balance and thinning at Eklutna Glacier, Alaska: an altitude-mass-balance feedback with implications for water resources. *Journal of Glaciology*, 63(238), 343-354.

Sass, L. C., O'Neel, S., Loso, M. G., MacGregor, J. A., Catania, G. A., & Larsen, C. F. (2009, December). Contributions of climate and dynamics to mass wastage and accumulation zone thinning of Eklutna Glacier, Alaska. In *AGU Fall Meeting Abstracts* (Vol. 1, p. 04).

Sass, L. C. (2011) *Characterizing Eklutna Glacier's response to climate through measurements of mass balance, geometry, and motion*. Diss. Alaska Pacific University.

Schulla, J., & Jasper, K. (2007). Model description wasim-eth. *Institute for Atmospheric and Climate Science, Swiss Federal Institute of Technology, Zürich*.

VanLooy, J., Foster, R., & Ford, A. (1998) Accelerating thinning of Kenai Peninsula glaciers, Alaska. *J. Glaciol.* 44, 570-582

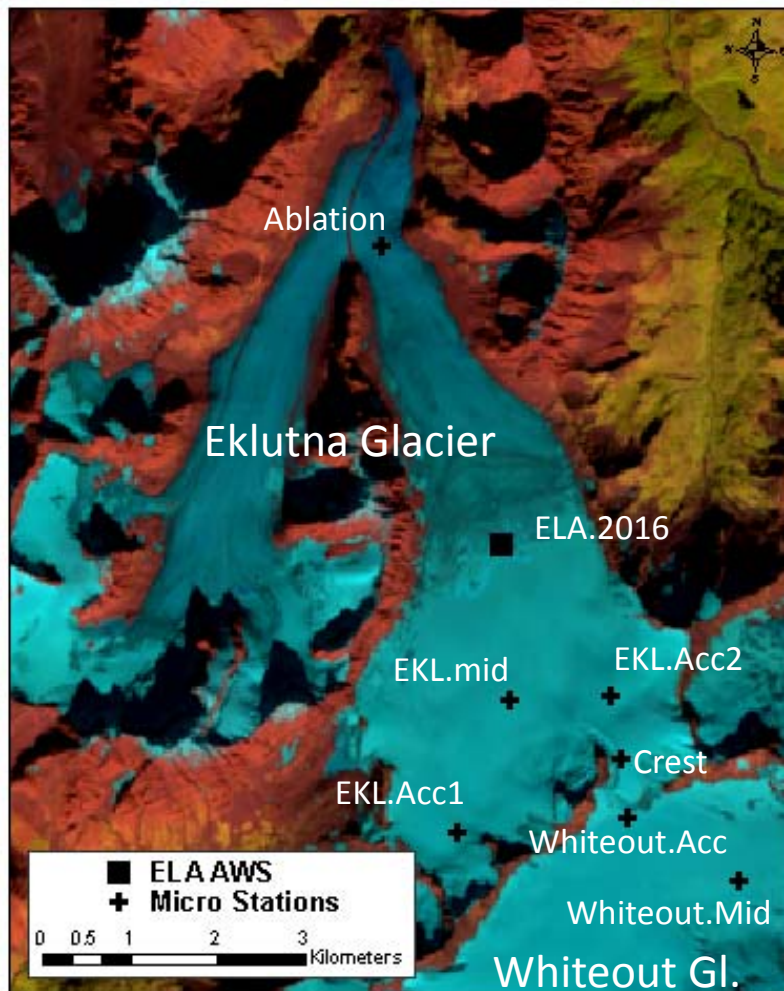


Figure 1. Study area showing locations of weather stations from Table 1.

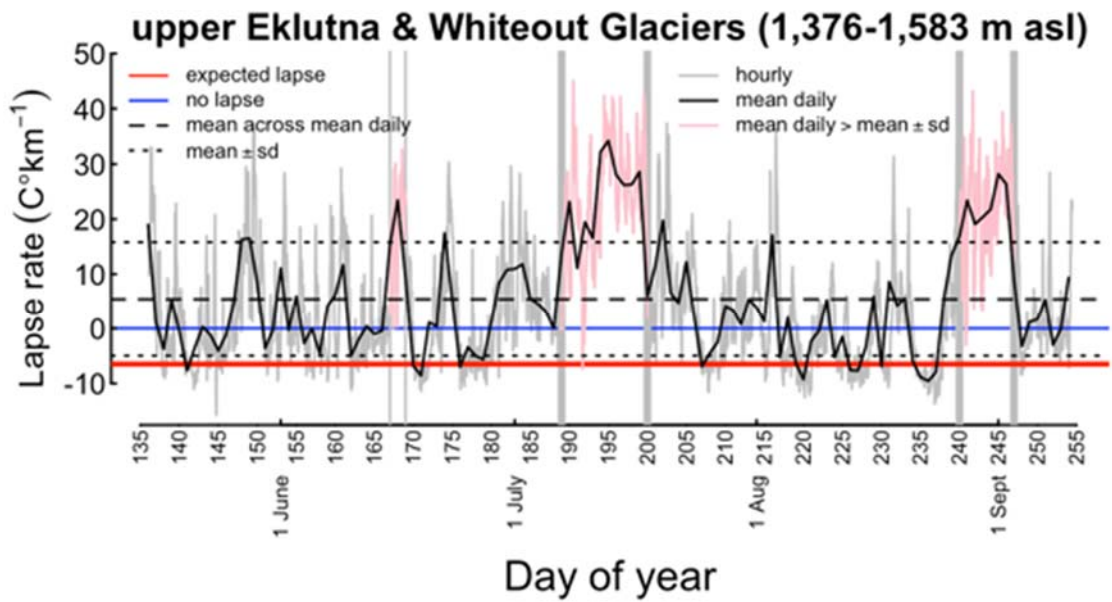
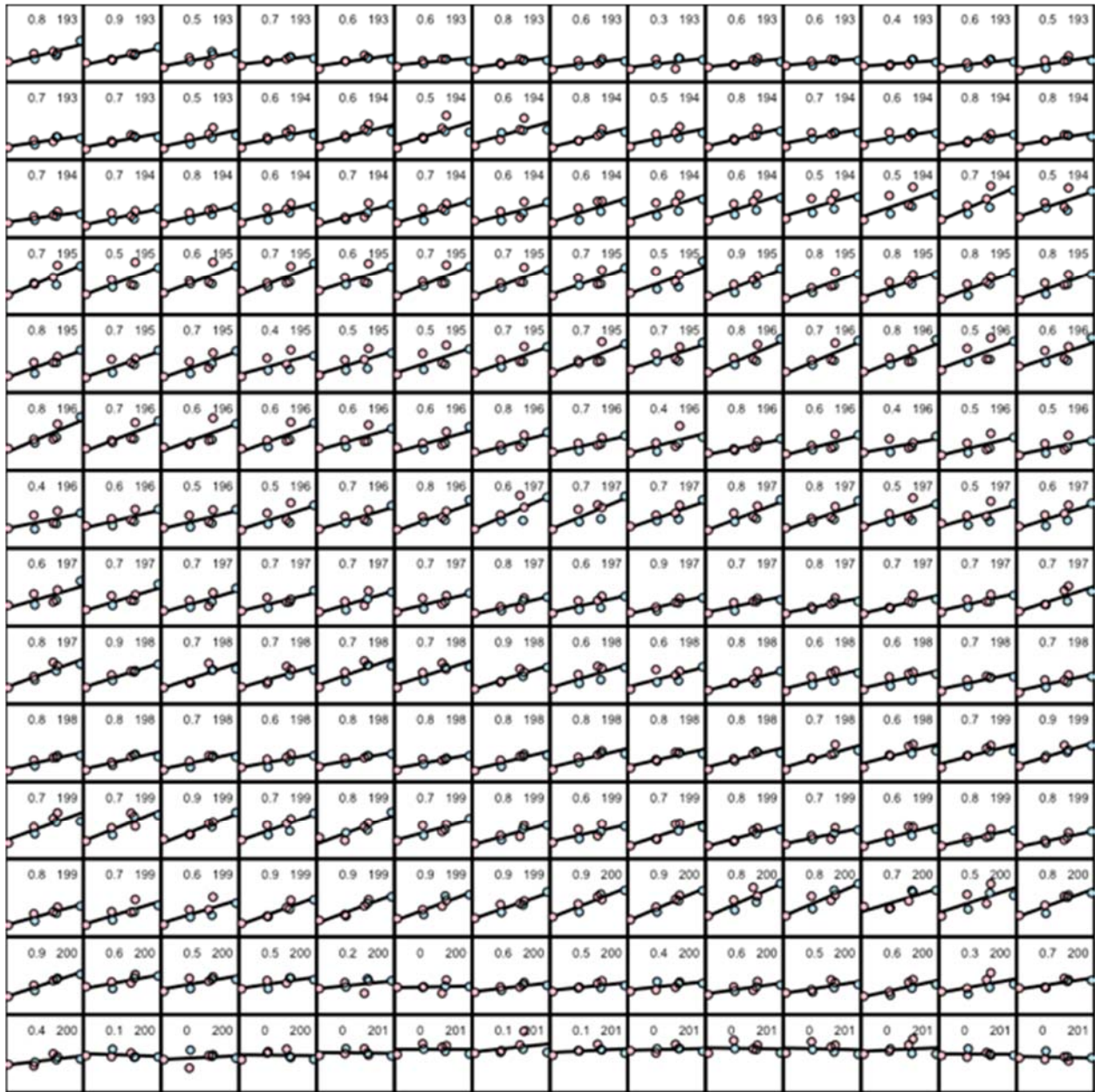


Figure 2. Lapse rates, L , over time, 15 May to 11 September 2016. Positive lapse rates above the horizontal blue line are inverted. Red line indicates $L_E = -6.5^\circ\text{C km}^{-1}$. Gray (and pink) time series is hourly lapse rate. Black solid line is mean daily lapse averaged across hours of a given day of year. Gray vertical lines and pink hourly lapse highlight period with lapse inversions greater than the mean daily lapse plus one standard deviation.



legend key

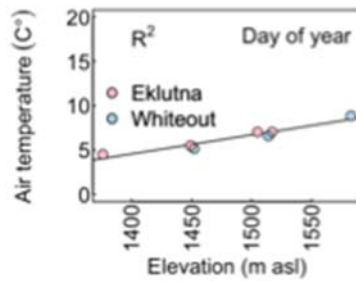


Figure 3. Temperature by elevation for period of very strong inversion in upper basins of Eklutna and Whiteout Glaciers, 11-19 July, 2016.

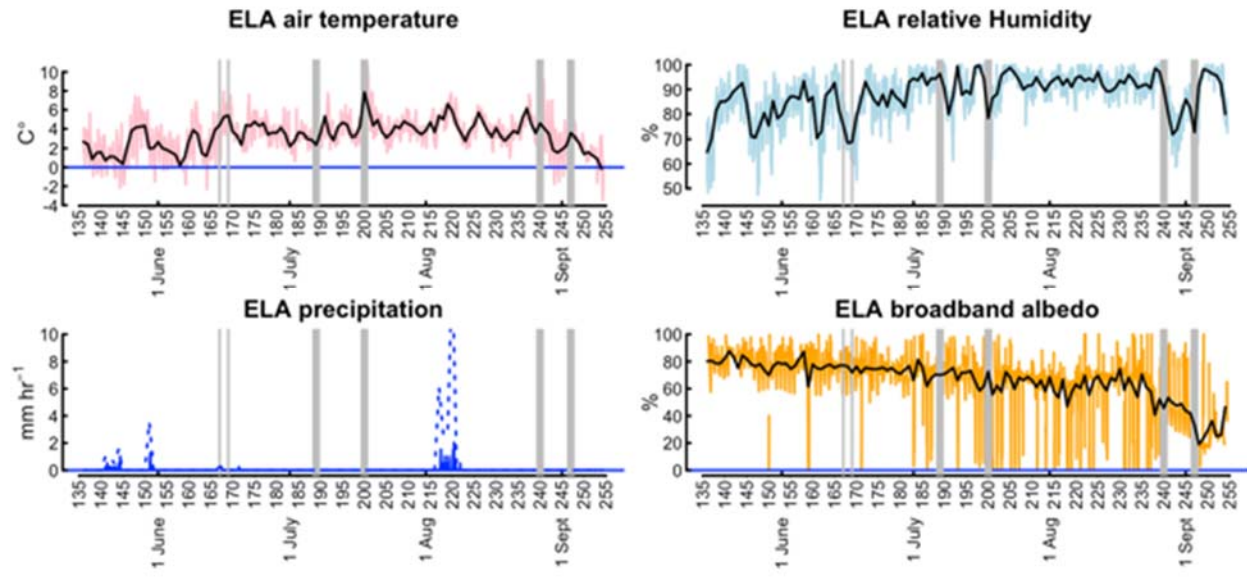


Figure 4. Standard meteorological variables from 15 May to 11 September at ELA.2016 station on Eklutna Glacier. Vertical gray lines correspond to time periods of very strong inversions shown in Fig. 2. ELA = ELA.2016 in Table 1.

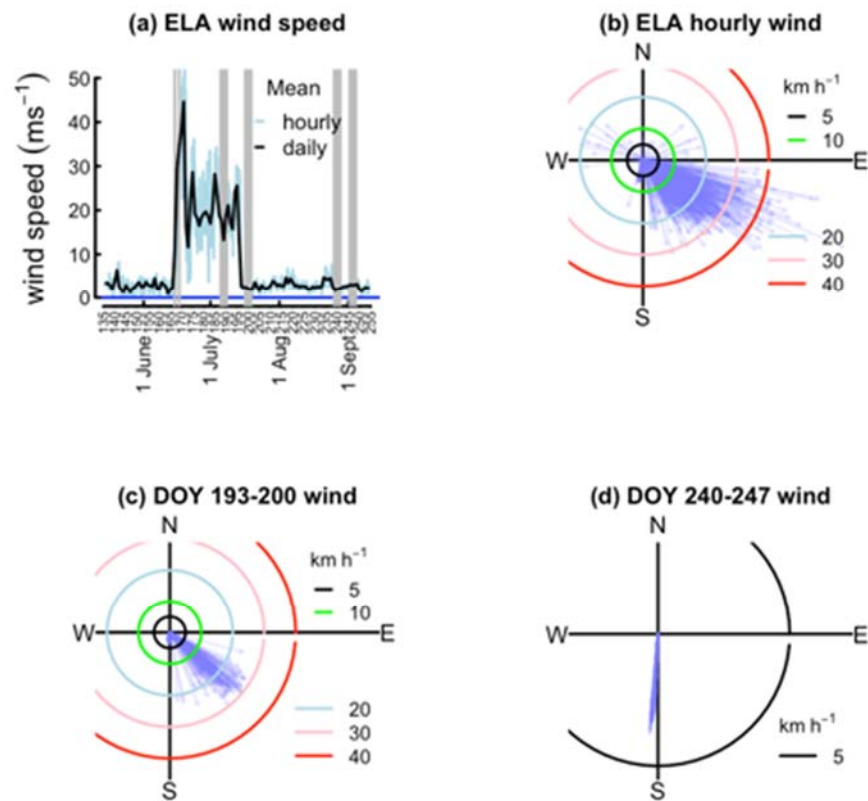


Figure 5. Wind speed and direction from ELA.2016 AWS. (a) Mean hourly (light blue) and mean daily (black) wind speed. Vertical gray lines show periods of strong inversions from Fig. 2. (b) Wind direction and strength (length of blue arrows) 15 June – 11 September. (c) Wind direction and speed during the strong mid-July and (d) late-August and early-September inversion periods. Note the change in wind speed scale in (d). ELA = ELA.2016 in Table 1.

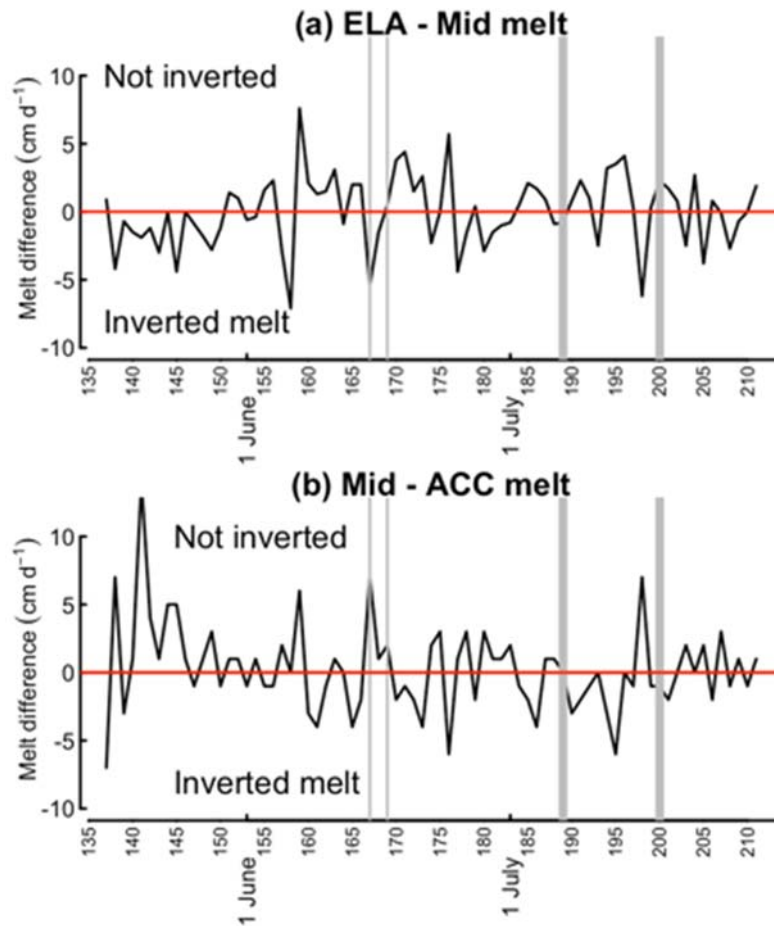


Figure 6. Melt inversions as differences between lower and upper elevation stations in Eklutna upper basin 15 May-28 July, 2016. Horizontal red line indicates no difference in melt between stations. Values above red line indicate the expected case of more melt at lower elevations (not inverted); values below red line indicate melt inversions. ELA. Vertical gray lines indicate strong temperature inversions shown in Fig. 2. ELA = ELA.2016, ACC = EKL.Acc2, and Mid = EKL.Mid in Table 1.

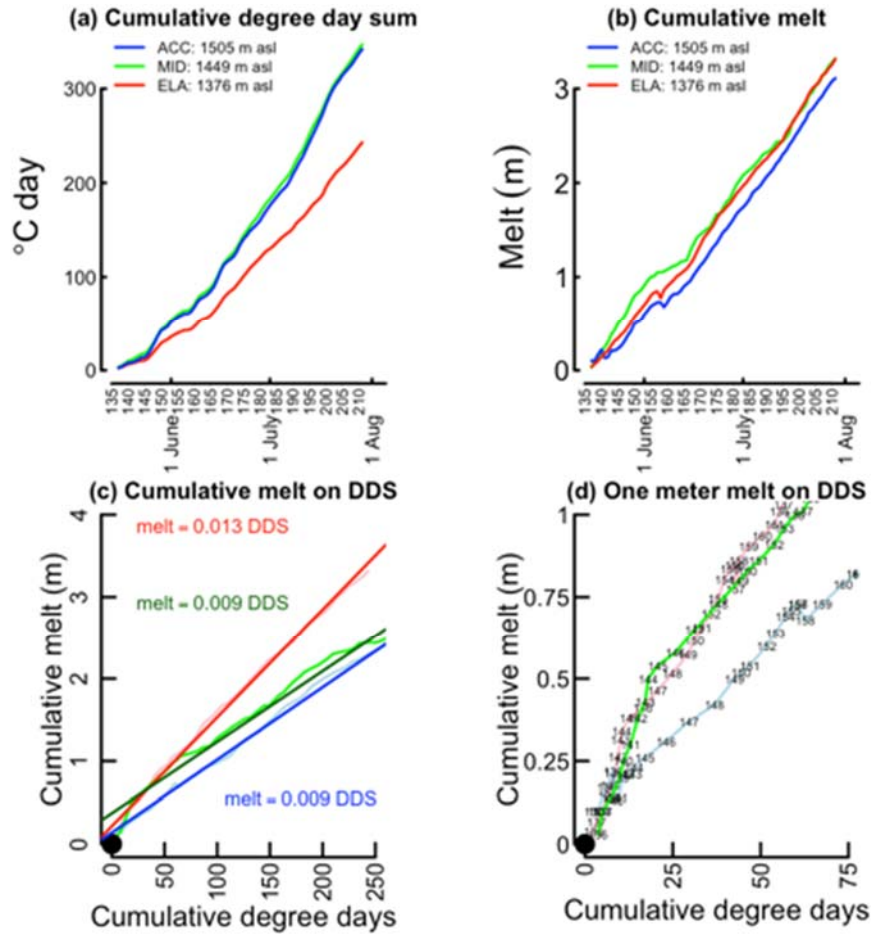


Figure 7. Cumulative melt variables at three stations on Eklutna Glacier 15 May-28 July, 2016. (a) Cumulative degree-day sum and (b) cumulative daily melt with stations indicated by color. (c) Cumulative daily melt, w , plotted against cumulative degree-day sum, dds , with best fit lines. Each line was fit with an intercept but legends show only slopes as degree-day factor, f , as $w = f dds$. (d) Same as (c) but only early time period, i.e., lower left corner of (c) with DOY indicated as numbers along plots. ELA = ELA.2016, ACC = EKL.Acc2, and Mid = EKL.Mid in Table 1.

Information Transfer Program Introduction

None.

USGS Summer Intern Program

None.

Student Support					
Category	Section 104 Base Grant	Section 104 NCGP Award	NIWR-USGS Internship	Supplemental Awards	Total
Undergraduate	2	0	0	0	2
Masters	5	0	0	0	5
Ph.D.	1	0	0	0	1
Post-Doc.	0	0	0	0	0
Total	8	0	0	0	8

Notable Awards and Achievements

The undergraduate student supported by this project (Stormy Fields) applied for and was awarded an URSA student grant to enhance her research experience during this research project. Stormy also presented a poster documenting her research experience through this project and main project findings at the undergraduate research day at UAF.

UAF Environmental Chemistry Symposium. Outstanding Graduate Presentation. Fairbanks, AK. April 21, 2017. USPA Student Travel Grant: Travel to American Geophysical Union Conference to present Transport of CH₄ in Open-Talik Lakes in Discontinuous Permafrost Aquifers, poster presentation. San Francisco, CA. December 12-16, 2016. AWRA-AK Grad Student Scholarship Competition Award. Proposal for research of Transport of Methane in Open-Talik Lakes in Discontinuous Permafrost Aquifers. April 26, 2016.